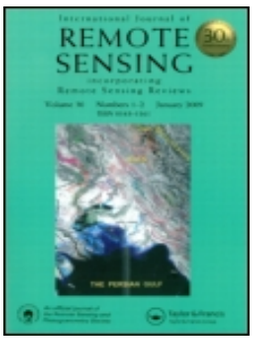

International Journal of Remote Sensing

ISSN: 0143-1161 (Print) 1366-5901 (Online) Journal homepage: http://www.tandfonline.com/loi/tres20

A wavelet domain detail compensation filtering technique for InSAR interferograms

Liang Chang , Xiufeng He & Jonathan Li

To cite this article: Liang Chang , Xiufeng He & Jonathan Li (2011) A wavelet domain detail compensation filtering technique for InSAR interferograms, International Journal of Remote Sensing, 32:23, 7985-7995, DOI: 10.1080/01431161.2010.531787

To link to this article: http://dx.doi.org/10.1080/01431161.2010.531787

Published online: 06 Oct 2011.

International Journal of Remote Sensing
Vol. 32, No. 23, 10 December 2011, 7985–7995

Taylor & Francis
Taylor & Francis Group

A wavelet domain detail compensation filtering technique for InSAR interferograms

LIANG CHANG†, XIUFENG HE*† and JONATHAN LI†‡
†Institute of Satellite Navigation and Spatial Information Systems, Hohai University, Nanjing, Jiangsu 210098, China
‡Department of Geography and Environmental Management, University of Waterloo, Waterloo, ON, Canada, N2L 3G1

(*Received 13 May 2010; in final form 30 August 2010*)

The quality of interferogram filtering affects the accuracy of interferometric synthetic aperture radar (InSAR) applications. This article presents a new wavelet domain filtering method for phase noise reduction in an InSAR interferogram. The method first transforms the real and imagery parts of the original interferogram into the wavelet domain using the stationary wavelet transform (SWT). Then the coefficients for each sub-band are filtered with detail compensation. Finally, the wavelet coefficients are reconstructed in the space domain by the inverse SWT. The results show that the proposed method can suppress the speckle effectively, maintain details of the interferogram well, and greatly reduce the number of residues.

1. Introduction

Interferometric synthetic aperture radar (InSAR) techniques, which use images acquired by two repeat passes over the same area, are being used increasingly to monitor landslides and volcanic deformation (Lundgren *et al.* 2001, Ohkura and Shimada 2001). During the past two decades, significant progress has been made in further developing differential InSAR (DInSAR) technology for earthquakes (Massonnet *et al.* 1993), ground movements (Fruneau *et al.* 1996, Usai 2001), volcanic eruptions (Massonnet *et al.* 1995, Webley *et al.* 2002), etc. However, the phase noise in the interferogram interferes with the phase unwrapping process and affects the quality of deformation information extracted from the interferogram. Furthermore, the contaminated fringes (lines of discontinuity due to phase wrapping) in the interferogram make simple linear low-pass filtering techniques inoperative (Sethu *et al.* 2008). Therefore, it is important to design a filter that can reduce noise effectively for applications of the interferogram.

Many techniques have been developed to reduce interferometric phase noise. The Frost filter (Frost *et al.* 1982) is an adaptive and exponentially weighted averaging filter based on the ratio of the local standard deviation to the local mean of the degraded image. Both pivoting mean filtering (Eichel *et al.* 1996) and pivoting median filtering (Lanari *et al.* 1996) are simple sliding-window spatial filters. Based on 16 directional

*Corresponding author. Email: xfhe@hhu.edu.cn

International Journal of Remote Sensing
ISSN 0143-1161 print/ISSN 1366-5901 online © 2011 Taylor & Francis
http://www.tandf.co.uk/journals
http://dx.doi.org/10.1080/01431161.2010.531787

masks to adaptively filter noise, the Lee filter was developed to preserve phase gradient and reduces phase noise according to the coherence (Lee *et al.* 1998). A modification of the Lee adaptive complex filter was proposed by Wu *et al.* (2006) to remove the limitation of the stationary orientation angle of the filtering window. The Boxcar filter was implemented on a rectangular window by Goldstein and Werner (1998). The Goldstein filter (Goldstein and Werner 1997) and the modified Goldstein filter (Baran *et al.* 2003) were used to solve this problem by using a frequency domain approach. Li *et al.* (2008) further modified the Goldstein filter by incorporating interferometric coherence and the look number. Yu *et al.* (2007) proposed an adaptive contoured window filter to remove the decorrelation noise from InSAR phase images. Other filtering techniques used for this purpose include the wavelet transform (López-Martínez and Fàbregas 2002, Zha *et al.* 2008) and fuzzy logic (Aiazzi *et al.* 2005). Meng *et al.* (2007) processed the InSAR interferogram on a nonlinear two-stage filter structure. Sethu *et al.* (2008) proposed a noise reduction technique using selective weighting of the wavelet coefficients of the noisy image. Li and Liao (2010) applied a method based on the minimum mean squared error (MMSE) criterion to auto-register the synthetic aperture radar (SAR) images together with reducing the interferometric phase noise simultaneously. However, there is a contradiction between speckle reduction and detail reservation in many current interferogram filters.

The InSAR interferogram phase can be represented in the time and frequency domains at the same time, and this can be realized by several solutions such as detrended fluctuation analysis (DFA) (Peng *et al*. 1994, Chen *et al*. 2002, Varotsos 2005a,b, Varotsos *et al.* 2005, Varotsos and Kirk-Davidoff 2006) and wavelet analysis (Fukuda and Hirosawa 1999, Audit *et al.* 2002, Valens 2004, Mallat 2008). DFA is capable of eliminating the non-stationarities in the interferogram (Chen *et al*. 2002). DFA has already proved its usefulness in several complex systems, such as surface air-pollutants (Varotsos *et al*. 2005), the total ozone content (Varotsos 2005a,b) and the global tropospheric temperature (Varotsos and Kirk-Davidoff 2006). In wavelet analysis the use of a fully scalable modulated window solves the signal-cutting problem. The window is shifted along the signal and the spectrum is calculated for every position. This process is then repeated many times with a slightly shorter (or longer) window for every new cycle. The final result is a collection of time–frequency representations of the signal, all with different resolutions (Valens 2004). A comparison between wavelet analysis and DFA can be found in Oświecimka *et al.* (2006). Wavelet analysis was chosen in this study because of its ease of implementation.

This article presents a novel wavelet domain detail compensation filtering method for phase noise reduction in InSAR interferograms. After decomposing an InSAR interferogram with wavelet analysis, the sub-band images are filtered with detail compensation. The idea of detail compensation is similar to the two-stage filter structure proposed by Meng *et al*. (2007). In our method, the interferogram is filtered twice. First, the three wavelet-decomposed high-frequency components of the interferogram are filtered with a facile filtering method (e.g. with the periodic pivoting mean filter (Eichel *et al.* 1996) or the periodic pivoting median filter (Lanari *et al.* 1996)) and then the difference interferogram can be obtained by subtracting the filtered interferogram from the original interferogram. Next, the difference interferogram is filtered again, and its outcome can be seen as the compensation to the original interferogram. Finally, the detail compensated filtered interferogram is obtained by adding the compensation to the filtered interferogram for the first time.

2. Principles of wavelet transform denoising

2.1 *The discrete wavelet transform*

The discrete wavelet transform (DWT) is a useful technique that can transform a discrete time signal to a discrete wavelet representation. Based on sub-band coding, it decomposes signals into basis functions through shifting and scaling:

$$X(t) = \sum_{m \in Z} \sum_{n \in Z} C_n^m \, \psi_{m,n}(t), \tag{1}$$

$$C_m^n = \left\langle X(t) \, \psi_{m,n}(t) \right\rangle, \tag{2}$$

$$\psi_{m,n}(t) = 2^{-m/2} \, \psi(2^{-m}x - n), \tag{3}$$

where $X(t)$ is the signal to be analysed, m and n are the pixel coordinates, C_m^n is the DWT coefficient, $\psi_{m,n}(t)$ is the wavelet function and $\langle \cdot \rangle$ denotes the inner products.

Multiresolution analysis is the design method of most of the practically relevant DWT and the justification for the algorithm of the fast wavelet transform (FWT). In a two-dimensional (2D) wavelet transform, mutiresolution analysis is carried out in row and column directions with a low-pass (L) and a high-pass (H) filter, decomposing the images and forming a pyramidal tree. During the decomposition, each (sub)image is downsampled by a factor of 2. An example is illustrated in figure 1 (Fukuda and Hirosawa 1999).

2.2 *The stationary wavelet transform*

The wavelet coefficients of DWT are sampled with scale change without violating the Nyquist criterion (Panda 2007). However, the classical DWT suffers a drawback: it is not time invariant. This means that, even with periodic signal extension, the DWT of a translated version of a signal X is not, in general, the translated version of the DWT of X. To preserve the invariance by translation, the down sampling operation

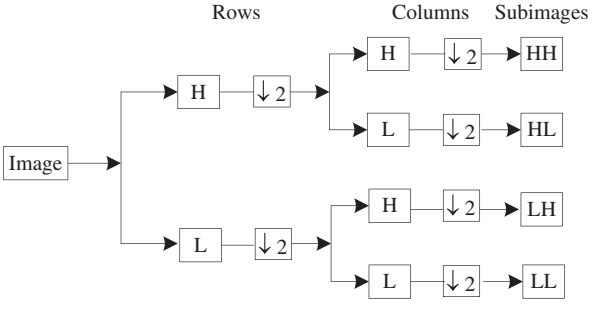

Figure 1. Wavelet decomposition of an image into four subimages. LL denotes the horizontal and vertical directions at low frequency; LH denotes the horizontal direction at low frequency together with the vertical direction at high frequency; HL denotes the horizontal direction at high frequency and the vertical direction at low frequency; and HH denotes the horizontal and vertical directions at high frequency. ↓ 2 denotes downsampling by a factor of 2.

must be suppressed and the decomposition obtained is then redundant and is called a stationary wavelet transform (SWT) (Mallat 2008).

3. The detail compensation filtering technique

3.1 *Detail compensation*

Some details of the interferogram will also be filtered out along with noise during the filtering process. To preserve as many details as possible, the idea of detail compensation is introduced. First, we filter the original interferogram and get the difference interferogram by subtracting the filtered interferogram from the original interferogram. Second, the difference interferogram is filtered for a second time with the purpose of compensation for lost details. Third, the filtered detail-compensated interferogram is obtained by adding the filtered difference interferogram in the second step to the filtered original interferogram in the first step.

In this article, to preserve the translation invariance during the wavelet transform and to compensate for the detail loss, the detail compensation is applied to the SWT decomposed high-frequency sub-bands.

3.2 *Realization of the detail compensation filter*

The practical procedure for the wavelet domain detail compensation filtering method for an InSAR interferogram consists of the following steps (see figure 2).

(1) Decompose the real and imaginary parts of the InSAR interferogram into four sub-bands using SWT, respectively.

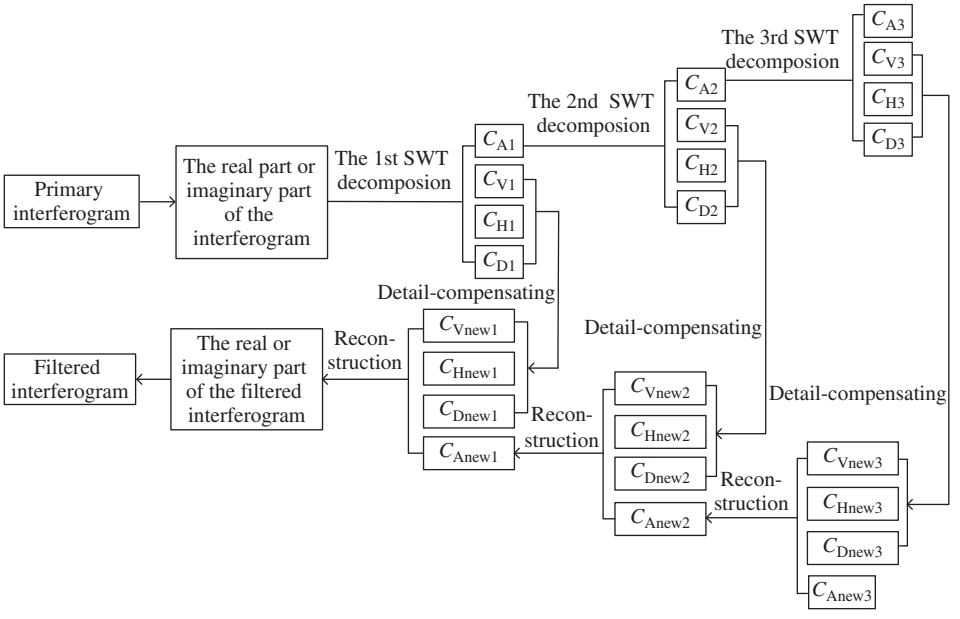

Figure 2. The flowchart of the wavelet domain detail compensation filtering method for an InSAR interferogram.

(2) All of the high-frequency sub-bands for each wavelet subspace are filtered with detail compensation. The high-frequency component D is filtered by some facile filtering method to get D', and the difference component ΔD is given by

$$\Delta D = W\left(D - D'\right), \tag{4}$$

where W is an operator to wrap real values to the principal interval $[-\pi, \pi)$. The difference component ΔD is then filtered again by the facile filtering method to get D'. Finally we obtain the compensated high-frequency component:

$$D_{\text{new}} = W\left(D' - D''\right). \tag{5}$$

During the filtering process, the size of the filtering windows at each wavelet level is defined as

$$w_i = w_0 2^{i-1} - 1, i \geq 2, \tag{6}$$

where $w_0 = 7$ denotes the size of the filtering window at the first level.

(3) Both the filtered real part and the imaginary part are reconstructed with the inverse SWT.

(4) The filtered interferogram with detail compensation is obtained by extracting the phase value from the reconstructed real and imaginary parts.

Figure 2 shows the flowchart of the detail compensation interferogram filtering method based on the SWT. $C_{\text{A}j}$, $C_{\text{V}j}$, $C_{\text{H}j}$ and $C_{\text{D}j}$ ($j = 1, 2, 3$) refer to the low-frequency components, high-frequency components in the vertical direction, high-frequency components in the horizontal direction and high-frequency components in the diagonal direction for each wavelet subspace, respectively. $C_{\text{Vnew}j}$, $C_{\text{Hnew}j}$ and $C_{\text{Dnew}j}$ ($j = 1, 2, 3$) refer to the high-frequency components for each wavelet subspace after detail compensation in the directions explained above.

4. Experimental results

The European remote sensing satellite (ERS) tandem images in single look complex (SLC) CEOS format acquired on 2 and 3 January 1996 over the city of Zhengjiang, Jiangsu, China (Track 00318/Orbit 23352 and 03679) were used to generate a interferogram of size 256 × 256. The SAR images were processed with GAMMA Remote Sensing software (GAMMA Remote Sensing Research and Consulting AG, Gümligen, Switzerland; http://www.gamma-rs.ch/) using the two-pass differential interferometric approach. The phase trend expected for a smooth curved Earth was removed from the interferogram, and then the flattened interferogram was obtained, as shown in figure 3(*a*).

To evaluate the performance of the proposed method, the interferogram was filtered with a two-stage filter structure (Meng *et al*. 2007), a Lee filter (Lee *et al.* 1998), Frost filter (Frost *et al.* 1982), Boxcar filter (Goldstein and Werner 1998), wavelet packet transform and a Wiener filter (Zha *et al*. 2008) and a selective weighting filter (Sethu *et al*. 2008) (figure 3(*b*)–(*g*)). Moreover, to test the validity of the detail compensation and the SWT-based methods, comparisons between DWT- and SWT-based methods were made, as well as those between detail compensation and non-detail compensation methods (figure 3(*h*)–(*k*)).

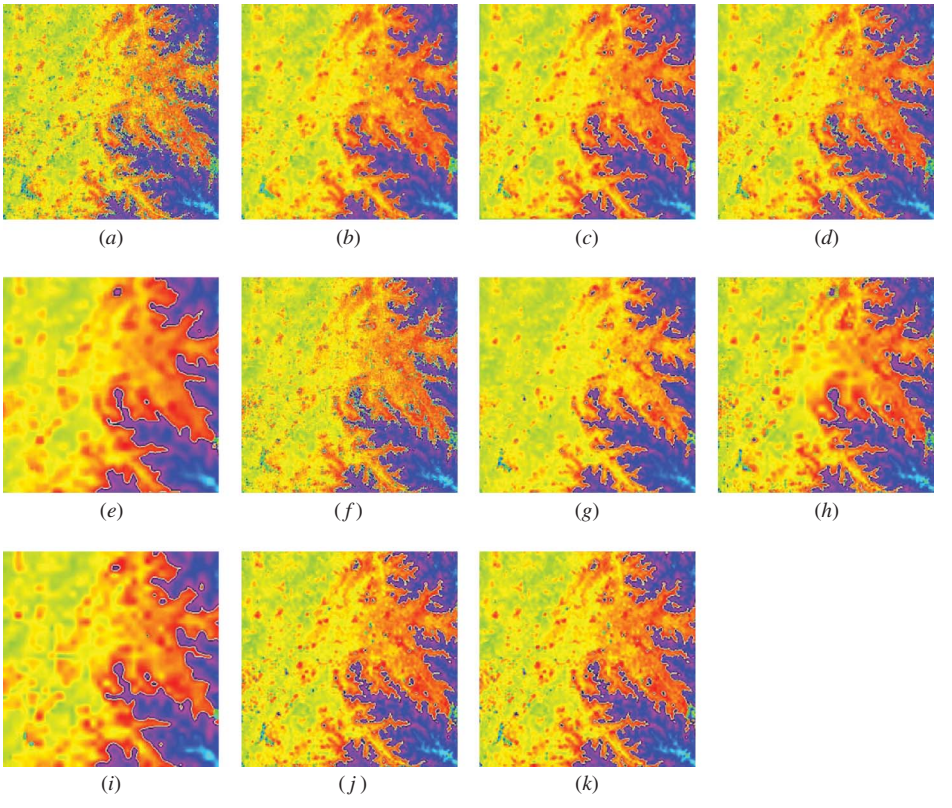

Figure 3. Comparison of (*a*) the original interferogram and (*b*)–(*k*) the filtered interferograms, using: (*b*) a two-stage filter structure, (*c*) a Lee filter, (*d*) a Frost filter, (*e*) a Boxcar filter, (*f*) the wavelet packet transform and a Wiener filter and (*g*) a selective weighting filter; a periodic pivoting mean filter based on DWT (*h*) without and (*i*) with detail compensation; and a periodic pivoting mean filter based on SWT (*j*) without and (*k*) with detail compensation.

From figure 3(*b*)–(*g*) it can be seen that the edge of the interferogram filtered by the Lee filter (figure 3(*c*)) is distorted, and that the Boxcar filter results in an over-smoothed image (figure 3(*e*)). Figure 3(*f*) shows that the interferogram generated by the wavelet packet transform and the Wiener filter cannot remove the residues effectively. Moreover, the image in figure 3(*g*) reveals that the selective weighting filter loses some details. Figure 3(*h*) shows that the periodic pivoting mean filter based on DWT can remove most of the noise, but there exist many residues near the edge of the image. Figure 3(*i*), like figure 3(*e*), is also over-smoothed. By comparing the SWT-based methods with the DWT-based methods, it can be concluded that the former perform better than the latter.

However, it is difficult to evaluate the performances of figure 3(*b*), (*d*) and (*k*). To show the comparisons more clearly, profiles (the second column in azimuth direction is chosen) along the range direction of the interferograms were extracted and are shown in figure 4. From the comparisons of figure 4(*b*), (*d*) and (*k*), it can be seen that the profile in figure 4(*k*) has a few glitches as well as a few residues (table 1). The reason for the serious glitches in figure 4(*b*) may be that the second column in the

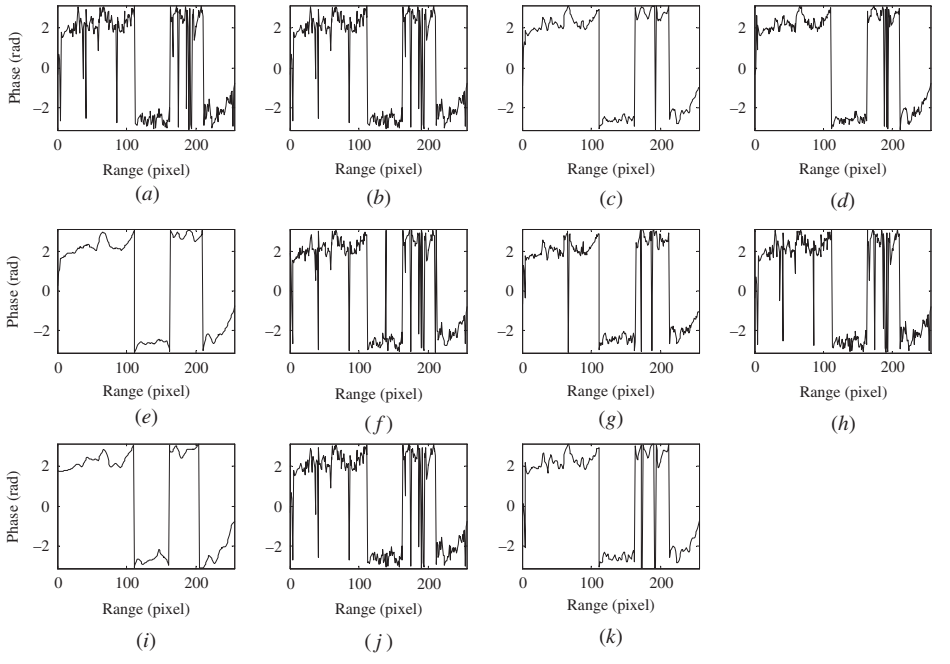

Figure 4. Comparison of profiles of (*a*) the original interferogram and (*b*)–(*k*) the filtered interferograms, using: (*b*) a two-stage filter structure, (*c*) a Lee filter, (*d*) a Frost filter, (*e*) a Boxcar filter, (*f*) the wavelet packet transform and a Wiener filter and (*g*) a selective weighting filter; a periodic pivoting mean filter based on DWT (*h*) without and (*i*) with detail compensation; and a periodic pivoting mean filter based on SWT (*j*) without and (*k*) with detail compensation.

azimuth direction occupies less than half of the filter's neighbourhood. Figure 4(*d*) relieves some of the glitches, but it is still worse than figure 4(*k*). Furthermore, the performances of figure 4(*e*) and (*i*) are consistent with previous analyses from figure 3(*e*) and (*i*), which show that both the Boxcar filter and the periodic pivoting mean filter based on DWT with detail compensation result in over-smoothed images. Thus, the comparisons from figures 3 and 4 reveal that the periodic pivoting mean filter based on SWT with detail compensation (figure 3(*k*)) performs better in both glitch mitigation and detail compensation.

The residues have a considerable impact on InSAR interferogram phase unwrapping, and the number of residues becomes an important indicator to measure the performances of interferogram filters. The numbers of residues of the original interferogram and the filtered interferograms are summarized in table 1. In addition, to evaluate the performances of the filtering algorithms, we used the universal image quality index (IQI) proposed by Wang and Bovik (2002) and the signal-to-noise ratio (SNR) and the mean square error (MSE). As shown in table 1, the SWT-based filters have more ideal IQI, SNR and MSE values than the DWT-based filters. The two-stage filter structure and selective weighting filter have similar indicators with the proposed technique, but they perform badly when the profiles along the range direction of the interferograms are compared.

Table 1. The number of residues, image quality index (IQI), mean square error (MSE) and signal-to-noise ratio (SNR) together with elapsed time for the original interferogram and interferograms generated by different filtering methods.

Method	No. of residues	IQI	MSE (rad)	SNR (dB)	Elapsed time (s)
Original	597	–	–	–	–
Two-stage filter structure	97	0.315	1.38	4.40	2.17
Lee filter	68	0.255	1.80	3.24	8.10
Frost filter	89	0.199	1.93	2.94	5.94
Boxcar filter	4	0.104	2.35	2.22	0.06
Wavelet packet transform and Wiener filter	157	0.606	1.07	5.53	5.38
Selective weighting filter	61	0.250	1.62	3.74	5.06
Periodic pivoting mean filter based on DWT	136	0.229	1.88	3.07	4.70
Periodic pivoting mean filter based on DWT with detail compensation	10	0.093	2.41	1.98	11.19
Periodic pivoting mean filter based on SWT	126	0.311	1.61	3.75	65.44
Periodic pivoting mean filter based on SWT with detail compensation	81	0.299	1.70	3.50	145.84

5. Conclusions

In this article, we have proposed a new InSAR interferogram filtering method. This method was presented by integrating the difference idea and the character of the SWT. Comparisons with the two-stage filter, Lee filter, Frost filter, Boxcar filter, wavelet packet transform and Wiener filter, selective weighting filter and the DWT-based filter are also made. The results of the study can be summarized as follows.

1. The proposed technique can overcome the drawback of the sliding-window spatial filters which distort the pixels that occupy less than half of the filter's neighbourhood.
2. By compensating for the InSAR interferogram details with the proposed method, it can effectively suppress the speckle, reduce the residues and maintain the details.
3. Compared with the detail compensation filters based on DWT, the detail compensation filters based on SWT perform better in both suppressing the speckle effectively and smoothing the interferogram moderately.

As the proposed technique is implemented in the wavelet domain and filtered with a facile filter, it is relatively expensive and complex to compute (see table 1). Further research will be directed towards improving the computational efficiency.

Acknowledgements
We are very grateful to the two anonymous referees for their constructive comments and valuable suggestions. This work was supported by the National Natural Science Foundation of China (Grant No. 40974001), the National Key Technology R&D

Programme of China (Grant No. 2008BAB29B01-6) and Fundamental Research Funds for the Central Universities (Grant Nos 2010B14514 and 2010B14714). Some figures in this article were generated with GMT software (Generic Mapping Tools software, Hawaii, USA; Wessel and Smith 1998).

References

Aiazzi, B., Baronti, S., Bianchini, M., Mori, A. and Alparone, L., 2005, Filtering of interferometric SAR phase images as a fuzzy matching-pursuit blind estimation. *EURASIP Journal on Applied Signal Processing*, **2005**, pp. 3220–3230.

Audit, B., Bacry, E., Muzy, J. and Arneodo, A., 2002, Wavelet-based estimators of scaling behavior. *IEEE Transactions on Information Theory*, **48**, pp. 2938–2954.

Baran, I., Stewart, M.P., Kampes, B.M., Perski, Z. and Lilly, P., 2003, A modification to the Goldstein radar interferogram filter. *IEEE Transactions on Geoscience and Remote Sensing*, **41**, pp. 2114–2118.

Chen, Z., Ivanov, P., Hu, K. and Stanley, H., 2002, Effect of nonstationarities on detrended fluctuation analysis. *Physical Review E*, **65**, p. 41107.

Eichel, P.H., Ghiglia, D.C., Jakowatz Jr., C.V., Thompson, P.A. and Wahl, D.E., 1996, *Spotlight SAR Interferometry for Terrain Elevation Mapping and Interferometric Change Detection*, Sandia National Laboratories Technical Report, No. 20, pp. 2539–2546 (Albuquerque, NM: Sandia National Laboratory).

Frost, V., Stiles, J., Shanmugan, K. and Holtzman, J., 1982, A model for radar images and its application to adaptive digital filtering of multiplicative noise. *IEEE Transactions on Pattern Analysis and Machine Intelligence*, **4**, pp. 157–166.

Fruneau, B., Achache, J. and Delacourt, C., 1996, Observation and modelling of the Saint-Etienne-de-Tinée landslide using SAR interferometry. *Tectonophysics*, **265**, pp. 181–190.

Fukuda, S. and Hirosawa, H., 1999, A wavelet-based texture feature set applied to classification of multifrequency polarimetric SAR images. *IEEE Transactions on Geoscience and Remote Sensing*, **37**, pp. 2282–2286.

Goldstein, R.M. and Werner, C., 1997, Radar ice motion interferometry. In *Proceedings of the 3rd ERS Symposium*, 17–21 March 1997, Florence, Italy. Compiled by T.D. Guyenne and D. Danesy (Paris: European Space Agency), Special Publication, Vol. 2, pp. 969–972.

Goldstein, R.M. and Werner, C.L., 1998, Radar interferogram filtering for geophysical applications. *Geophysical Research Letters*, **25**, pp. 4035–4038.

Lanari, R., Fornaro, G., Riccio, D., Migliaccio, M., Papathanassiou, K.P., Moreira, J.R., Schwabisch, M., Dutra, L., Puglisi, G., Franceschetti, G. and Coltelli, M., 1996, Generation of digital elevation models by using SIR-C/X-SAR multifrequency two-pass interferometry: the Etna case study. *IEEE Transactions on Geoscience and Remote Sensing*, **34**, pp. 1097–1114.

Lee, J.S., Papathanassiou, K.P., Ainsworth, T.L., Grunes, M.R. and Reigber, A., 1998, A new technique for noise filtering of SAR interferometric phase images. *IEEE Transactions on Geoscience and Remote Sensing*, **36**, pp. 1456–1465.

Li, H. and Liao, G.S., 2010, An estimation method for InSAR interferometric phase based on MMSE criterion. *IEEE Transactions on Geoscience and Remote Sensing*, **48**, pp. 1457–1469.

Li, Z.W., Ding, X.L., Huang, C., Zhu, J.J. and Chen, Y.L., 2008, Improved filtering parameter determination for the Goldstein radar interferogram filter. *International Journal of Photogrammetry and Remote Sensing*, **63**, pp. 621–634.

López-Martínez, C. and Fàbregas, X., 2002, Modeling and reduction of SAR interferometric phase noise in the wavelet domain. *IEEE Transactions on Geoscience and Remote Sensing*, **40**, pp. 2553–2566.

Lundgren, P., Usai, S., Sansosti, E., Lanari, R., Tesauro, M., Fornaro, G. and Berardino, P., 2001, Modeling surface deformation observed with SAR interferometry at Campi Flegrei caldera. *Journal of Geophysical Research*, **106**, pp. 19355–19366.

Mallat, S., 2008, *A Wavelet Tour of Signal Processing*, 3rd ed. (San Diego, CA: Academic Press).

Massonnet, D., Briole, P. and Arnaud, A., 1995, Deflation of Mount Etna monitored by spaceborne radar interferometry. *Nature*, **375**, pp. 567–570.

Massonnet, D., Rossi, M., Carmona, C., Adragna, F., Peltzer, G., Feigl, K. and Rabaute, T., 1993, The displacement field of the Landers earthquake mapped by radar interferometry. *Nature*, **364**, pp. 138–142.

Meng, D., Sethu, V., Ambikairajah, E. and Ge, L.L., 2007, A novel technique for noise reduction in InSAR images. *IEEE Geoscience and Remote Sensing Letters*, **4**, pp. 226–230.

Ohkura, H. and Shimada, M., 2001, InSAR analysis of Miyakejima volcano with RADARSAT images. In *Proceedings of the International Symposium of the International Geoscience and Remote Sensing Symposium*, 9–13 July 2001, Sydney, Australia (Piscataway, NJ: IEEE Operations Center), vol. 7, pp. 3001–3005.

Oświecimka, P., Kwapień, J. and Drozdz, S., 2006, Wavelet versus detrended fluctuation analysis of multifractal structures. *Physical Review E*, **74**, 016103, doi: 10.1103/PhysRevE.74.016103.

Panda, D., 2007, Eye detection using wavelets and ANN. Bachelor thesis, National Institute of Technology, Rourkela, Orissa, India.

Peng, C., Buldyrev, S., Havlin, S., Simons, M., Stanley, H. and Goldberger, A., 1994, Mosaic organization of DNA nucleotides. *Physical Review E*, **49**, pp. 1685–1689.

Sethu, V., Ambikairajah, E. and Ge, L.L., 2008, Selective weighting of undecimated wavelet coefficients for noise reduction in SAR interferograms. *EURASIP Journal on Advances in Signal Processing*, **2008**, pp. 78092–78099.

Usai, S., 2001, A new approach for long term monitoring of deformations by differential SAR interferometry. PhD thesis, Delft University of Technology, Delft, the Netherlands.

Valens, C., 2004, A really friendly guide to wavelets. Available online at: http://polyvalens.pagesperso-orange.fr/clemens/wavelets/wavelets.html (accessed 28 August 2010).

Varotsos, C., 2005a, Modern computational techniques for environmental data: application to the global ozone layer. In *Computational Science – ICCS 2005, Lecture Notes in Computer Science*, **3516**, pp. 504–510 (Berlin: Springer).

Varotsos, C., 2005b, Power-law correlations in column ozone over Antarctica. *International Journal of Remote Sensing*, **26**, pp. 3333–3342.

Varotsos, C. and Kirk-Davidoff, D., 2006, Long-memory processes in ozone and temperature variations at the region 60° S–60° N. *Atmospheric Chemistry and Physics*, **6**, pp. 4093–4100.

Varotsos, C., Ondov, J. and Efstathiou, M., 2005, Scaling properties of air pollution in Athens, Greece and Baltimore, Maryland. *Atmospheric Environment*, **39**, pp. 4041–4047.

Wang, Z. and Bovik, A.C., 2002, A universal image quality index. *IEEE Signal Processing Letters*, **9**, pp. 81–84.

Webley, P., Bingley, R., Dodson, A., Wadge, G., Waugh, S. and James, I., 2002, Atmospheric water vapour correction to InSAR surface motion measurements on mountains: results from a dense GPS network on Mount Etna. *Physics and Chemistry of the Earth*, **27**, pp. 363–370.

Wessel, P. and Smith, W.H.F., 1998, New, improved version of generic mapping tools released. *EOS, Transactions American Geophysical Union*, **79**, p. 579.

Wu, N., Feng, D.Z. and Li, J. X., 2006, A locally adaptive filter of interferometric phase images. *IEEE Geoscience and Remote Sensing Letters*, **3**, pp. 73–77.

Yu, Q.F., Yang, X., Fu, S.H., Liu, X.L. and Sun, X.Y., 2007, An adaptive contoured window filter for interferometric synthetic aperture radar. *IEEE Geoscience and Remote Sensing Letters*, **4**, pp. 23–26.

Zha, X.J., Fu, R.S., Dai, Z.Y. and Liu, B., 2008, Noise reduction in interferograms using the wavelet packet transform and Wiener filtering. *IEEE Geoscience and Remote Sensing Letters*, **5**, pp. 404–408.